International Journal of Earth Sciences
https://doi.org/10.1007/s00531-025-02520-3

ORIGINAL PAPER

CO_2, ^{222}Rn, and He degassing from hydrothermal springs on the cone of Mt. Changbai with implications for volcano monitoring

Le Hu[1,2] · Xiaodong Pan[3] · Guangpei Zhong[3] · Guohui Gu[1,3] · Zhaofei Liu[1,2] · Ying Li[1,2] · Mengmeng Li[1,3]

Received: 27 February 2025 / Accepted: 27 June 2025

Abstract

Mt. Changbai volcano, one of the largest and most hazardous active volcanoes in the world, poses destructive threats to neighboring communities and thus should be monitored proactively. The analysis of bubbling gases in volcanic hydrothermal systems offers valuable insights into subsurface magmatic activities and serves as a critical tool in global volcano surveillance. There are two hydrothermal group springs named Julong Springs and Jinjiang Springs on the Mt. Changbai cone of which the gas geochemistry should be further investigated before efficient monitoring strategies are proposed. Here, chemical and isotopic characteristics of degassing CO_2, ^{222}Rn, and He from the two springs are systematically investigated. The results show that these two springs exhibit similar C–He isotopic signatures typically of magmatic provenance while they are largely different in gas compositions and fluxes. The Julong Springs exhibit significantly higher CO_2 and radon concentrations coupled with elevated radon flux compared to the Jinjiang Springs. However, He concentration and CO_2 flux at the Julong Springs are depleted relative to the Jinjiang Springs, which are diagnostic signatures of residual degassing. In combination with previous geophysical data, we believe that excess ^{222}Rn at the Julong Springs is sourced from a shallow-crustal magma pocket given ^{222}Rn's short half-life. Such a pocket is decoupled from its main magma chamber at present due to the lack of recharges, and the degassing intensity is receding gradually as the magma cools down. However, the emitted gases at the Jinjiang Springs originate directly from the main magma chamber with a larger volume of magma and more extensive magmatism. Therefore, gas geochemistry of the two springs on Mt. Changbai volcano can be a distinctive tool to identify subsurface magmatic activities at the different depths. The integrated monitoring at both sites enables dynamic assessment of magmatic unrest processes and enhances eruption forecasting capabilities. The findings highlight the necessity of conducting volcanic gas geochemistry investigations prior to the application of gas monitoring.

Keywords Carbon dioxide · Radon · Helium · Magmatic degassing · Mount Changbai volcano

Introduction

Monitoring large volcanoes with eruptive potential facilitates the implementation of advanced preparedness measures, thereby reducing disaster risks (Tilling 2008; Cassidy and Mani 2022). For active volcanoes at quiescent stages, their revival and re-eruption processes are controlled by the physical–chemical states of magma reservoirs, including temperature, volatile content, and crystallinity (e.g., Bachmann and Bergantz 2008; Chiodini et al. 2016). The injection of hot, volatile-rich, and low-viscosity mantle-sourced magma can reactivate stagnant and crystal-rich upper-crustal magma reservoirs through thermal perturbation, pressurization, and consequent remobilization processes (Patanè et al. 2003; Ruprecht and Bachmann 2010; Mangler et al. 2022). Thus, timely recognition of magmatic unrest signals is a

✉ Le Hu
hulecugb@126.com

✉ Xiaodong Pan
panxd1970@126.com

[1] Institute of Earthquake Forecasting, China Earthquake Administration, Beijing, China

[2] Key Laboratory of Earthquake Forecasting and Risk Assessment, Ministry of Emergency Management, Beijing, China

[3] Jilin Changbaishan Volcano National Observation and Research Station, Jilin Earthquake Agency, Changchun, China

Published online: 09 July 2025

key for the effective monitoring of an active volcano. However, at present, detecting such signals remains a significant challenge for worldwide volcano monitoring, particularly in terms of cost efficiency and observational timeliness (Ferres et al. 2015). In this context, near-surface geochemical monitoring of hydrothermal gases has proven to be an effective and widely adopted approach (e.g., Huppert and Woods 2002; Aiuppa et al. 2021), offering the advantages of continuous monitoring capabilities and cost-effectiveness. During pre-eruptive phases, microcracks develop in the magma chamber's country rocks, facilitating the migration of magmatically derived volatiles. These volatile components subsequently infiltrate the hydrothermal system and ascend to the surface, inducing measurable variations in surface gas geochemistry (concentrations, fluxes, and isotopes).

Mount Changbai/Paektu volcano (Herein after Mt. Changbai) is a large and one of the most explosive volcanoes in the world. It has a great importance and urgency to perform an effective monitoring. There are two major hydrothermal group spring named Julong Springs and Jinjiang Springs (hereinafter JLS and JJS, respectively) with continuous bubbling gas on the volcanic cone of China side, which are accessible to be monitored and which may potentially provide the signs of deep magmatism (Wei et al. 2021). To identify the origin/s of those two group springs, in the present study, concentrations, fluxes, and isotopes of CO_2, ^{222}Rn (Herein after Rn), and He emitted from JLS and JJS are analyzed, respectively, and their links to volcanic magmatism are investigated. Based on these results, different monitoring strategies are proposed.

Geological background

Mt. Changbai volcano (Fig. 1), located on the border area between China and North Korea, is genetically related to the westward subduction of the Pacific plate (Zhang et al. 2018). It is 2744 m tall with a large caldera containing a 384 m deep lake called "Tianchi" (Fig. 1b). The volcano has experienced three important evolutionary periods which are the basaltic shield-construction period in the Pliocene to Early Pleistocene (5–1 Ma), the cone-forming periods in

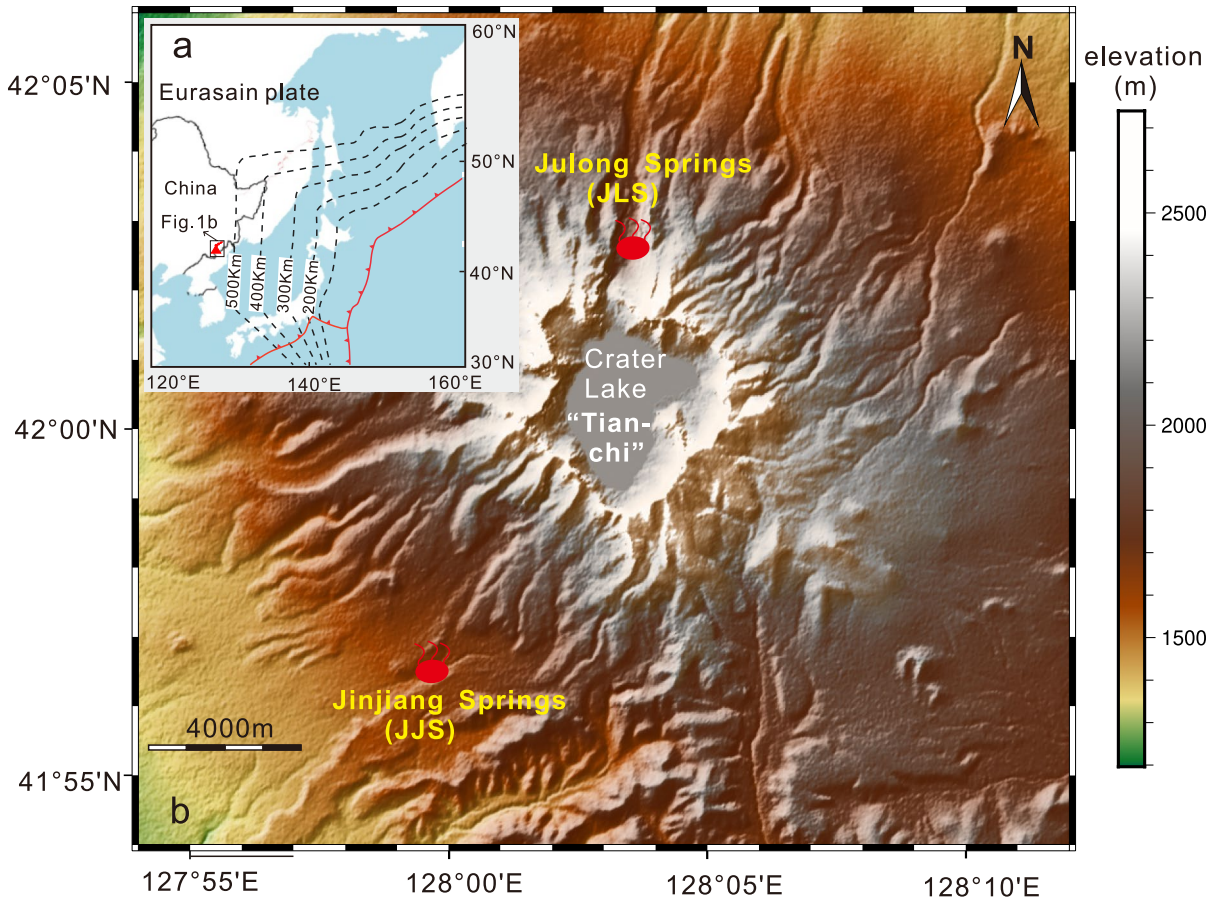

Fig. 1 Location and topography of Mt. Changbai volcano. **a** A sketch map shows the location of Mt. Changbai volcano. **b** Topographic map of Mt. Changbai volcano and sites of the hydrothermal springs

the Middle Pleistocene to Late Pleistocene (1–0.01 Ma), and the latest explosive eruptions period in the Holocene (Wei et al. 2013; Zhang et al. 2018; Pan et al. 2020). The most destructive eruption happened in ~ 1000 AD which led to the current topography of the volcano. The eruption reached a Volcanic Explosivity Index (VEI) of 7 and was one of the two largest eruptions in the last 2000 years (Zou et al. 2010; Oppenheimer et al. 2017). Notably, magmatic unrest occurred during the years 2002–2006 (Xu et al. 2012), which raised concerns and worries that the volcano would erupt again. This unrest event confirmed that the magmatic system remains active. Geophysical images have also shown the existence of high-conductivity and low-velocity reservoirs from the upper mantle to upper crust, which were interpreted as magma chambers or channels (e.g., Kim et al. 2017; Hammond et al. 2020; Fan et al. 2022). Therefore, Mt. Changbai volcano still has potential danger of eruption and requires enhanced surveillance.

Hydrothermal activities are abundant at Mt. Changbai volcano due to the heat source provided by magma. There are lots of bubbling hydrothermal springs concentrated in three main clusters on the cone area within China which are Lake Shoreline springs in the "Tianchi" crater lake, JLS on the north side, and JJS on the southwest side (Fig. 1b). The Lake Shoreline springs are inaccessible due to safety regulations established by local tourism authority, while JLS and JJS are available to be monitored at present. Temperature monitoring data since 2017 reported by Wei et al. (2021) show that JLS (70.2–75.2 °C) maintain relatively higher temperatures than JJS (50.0–64.5 °C). Both springs exhibit similar hydrological cycle and hydrochemical characteristics (Yan et al. 2018; Na et al. 2020). The geothermal reservoirs of these springs are inferred to be composed of fractured volcanic breccia, sandstone, and marble, whose cap rocks are trachyte, basalt, and rhyolitic and pyroclastic rocks (Yan et al. 2018). The spring waters are primarily recharged by atmospheric precipitation, and their hydrochemical type is Na-HCO_3 (Yan et al. 2018; Zhao et al. 2019). The average geothermal reservoir temperature and circulation depth are calculated to be 170 °C and 4.90 km for JLS and 162 °C and 4.67 km for JJS (Na et al. 2020).

Analytical methods

Bubbling gas samples from JLS and JJS were collected using the water draining method during the years 2021–2023. The customized sampling equipment consists of an inverted funnel and a gas collection glass column which is connected to a syringe and the funnel by rubber tubes at both ends. When sampling, the inverted funnel was submerged into spring water, and the syringe was used to empty the air trapped in the equipment completely and fill the column with water. Then let the accumulated spring bubbles enter into the glass column to displace water until it was filled with gas. The collected gas was finally injected into 500 mL pre-vacuumed aluminum bags for the laboratory analysis. The gas composition (CO_2, CH_4, N_2, and He) was analyzed at Mt. Changbai Volcano Observatory shortly after collection using an SP-3400 gas chromatograph of which the measurement uncertainty is less than ± 5 ‰. Some samples were also analyzed for isotopic measurements of carbon and helium at the Geo-analytical Center of Nuclear Industry, Beijing. $\delta^{13}C_{CO2}$ values were determined using a MAT 253 stable isotope ratio analysis system (with uncertainties of ± 0.3 ‰) and reported in per mil (‰) against the reference standard of Vienna Pee Dee Belemnite ($V\text{-}_{PDB}$). Helium and neon isotopes were analyzed using a Helix SFT noble gas mass spectrometer (Thermo-Fisher scientific, USA) with analytical errors within ± 3%.

Two hydrothermal springs with abundant bubbles at JLS and JJS were selected, respectively, for measurement of CO_2 and Rn degassing rate. The static closed chamber method (Chiodini et al. 1998) was employed. A hemispherical chamber with a radius of 0.2 m was used and connected to both the inlet and outlet of the gas detector via rubber tubes. An inlet filter and desiccant were used to avoid the dust and moisture. During sampling, the hemispherical chamber rim was fixed a little below the water surface covering the bubbling area. The CO_2 was detected by an infrared CO_2 analyzer (GXH-3010E) of which the detection limit is 0.01%. The Rn was measured by a RAD 7 detector with detection limit of 4 Bq/m^3. Gas flux is calculated by linear regression of the gas concentration accumulated in the chamber. Detailed methods are described in Liu et al. (2024).

Results

Chemical and isotopic compositions

Detailed chemical and isotopic data of hydrothermal gas analyzed in this study, along with data collected from literature, are listed in the Supplementary Material 1. CO_2 and N_2 concentrations range from 80.9 to 99.5% and 0.2–15.0% at JLS, and 73.36–94.9% and 2.3–22.1% at JJS. In combination with historical data, it is obvious that there is a negative correlation between CO_2 and N_2 (Fig. 2a), both at JLS and JJS. O_2 concentrations vary from 0.04 to 2.40% at JLS and 0.10–0.30% at JJS. As shown in Fig. 2b, N_2 and O_2 exhibit no relevance at JJS but a linear relationship at JLS with a slope matching the O_2/N_2 ratio (0.266) in the air, indicating that N_2 and O_2 at JLS are sourced mainly from the air. He concentrations are 6.6–31.1 ppm at JLS and 141.1–544.9 ppm at JJS. At JLS, He concentrations show no correlation with CO_2 and N_2 (Fig. 3a, b), whereas

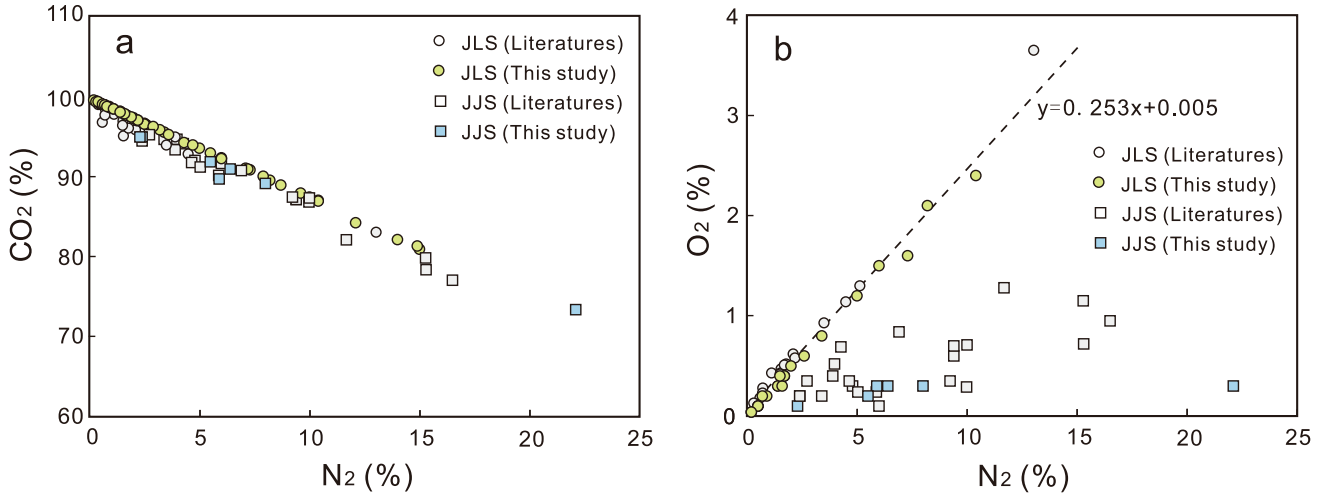

Fig. 2 Correlation diagrams of major gas compositions from JLS and JJS samples. **a** Scatter plots of N_2 versus CO_2 in both JLS and JJS samples showing a negative correlation. **b** Scatter plots of N_2 versus O_2 showing no correlation in JJS samples but a linear trend in JLS samples. The gray symbols represent data from literatures (Zhang et al. 2015; Wei et al. 2016; Gu et al. 2025)

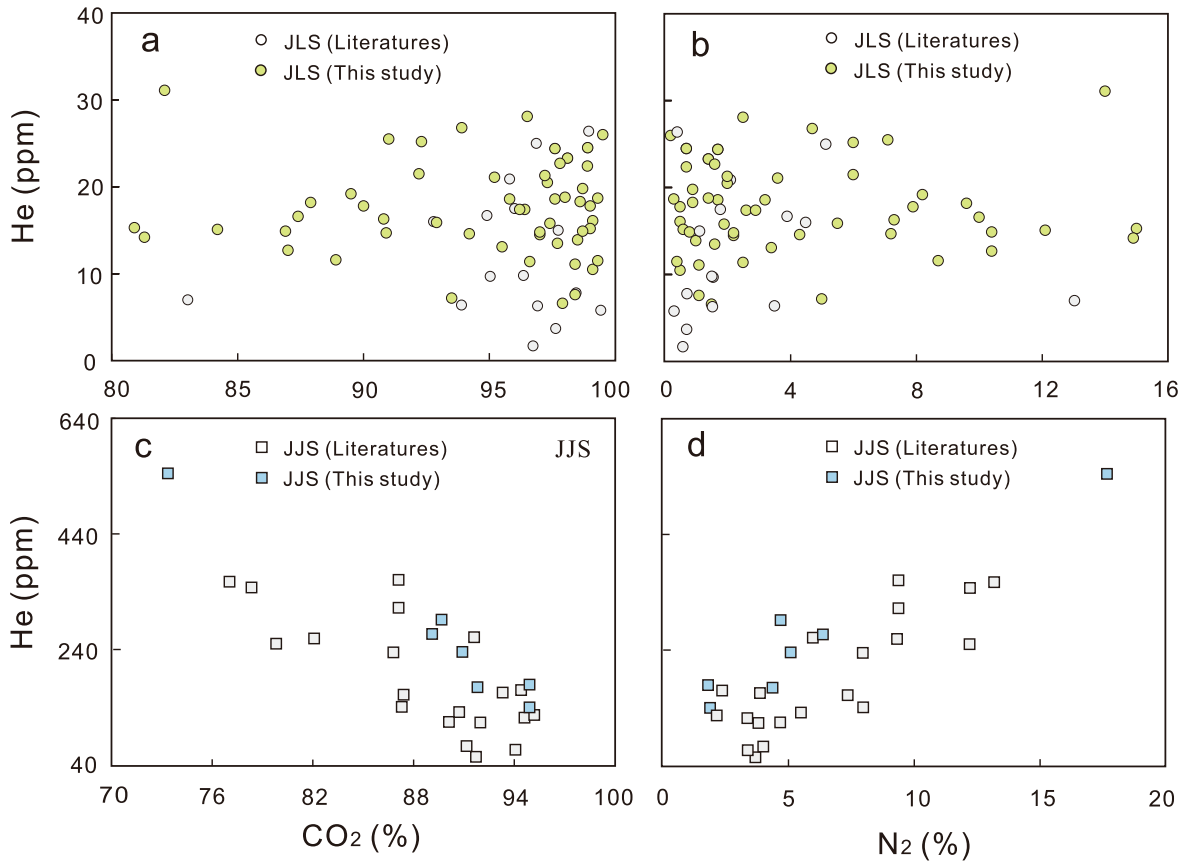

Fig. 3 Scatter diagrams of CO_2 versus He and N_2 versus He of gas samples from JLS and JJS. **a** Scatter plots of CO_2 versus He in JLS samples showing no correlation. **b** Scatter plots of N_2 versus He in JLS samples showing no correlation. **c** Scatter plots of CO_2 versus He in JJS samples showing a negative correlation. **d** Scatter plots of N_2 versus He in JJS samples showing a positive correlation. The gray symbols represent data from literatures (Zhang et al. 2015; Wei et al. 2016; Gu et al. 2025)

at JJS, significant correlations exist (Fig. 3c, d), implying a common source for CO_2, N_2, and He at JJS. $\delta^{13}C_{CO2}$ values range from − 4.87 to − 7.90 ‰ at JLS and − 5.11 to − 9.0‰ at JJS. $^3He/^4He$ ratios are 5.25 Ra at JLS and 5.38 Ra at JJS, where Ra represents the atmospheric $^3He/^4He$ ratio (1.39×10^{-6}, Mamyrin and Tolstikhin 1984). Both $\delta^{13}C_{CO2}$ and $^3He/^4He$ ratios obtained in this study align with previews reports (Zhang et al. 2015; Wei et al. 2016; Gu et al. 2025).

CO_2 and Rn fluxes

Real-time measured values of degassing CO_2 and Rn concentration in the hemispherical chamber are provided in the Supplementary Material 2. Their temporal variations are shown in Fig. 4. The data reveal that the CO_2 accumulation rates at JLS are significantly lower than at JJS (Fig. 4a), but the opposite trend is observed for Rn accumulation (Fig. 4b). Calculated fluxes of CO_2 at JLS and JJS are 10.07 kg m^{-2} day^{-1} and 29.24 kg m^{-2} day^{-1}, respectively, whereas of Rn are 27.36 Bq m^{-2} s^{-1} at JLS and 22.56 Bq m^{-2} s^{-1} at JJS. Although Rn concentration cannot be analyzed directly by gas chromatography, the saturation concentration during flux measurement can effectively represent the Rn concentration released from hydrothermal springs. Figure 4b shows that the saturation concentration at JLS is about 320 K Bq m^{-3}, much high than at JJS which is about 120 K Bq m^{-3}.

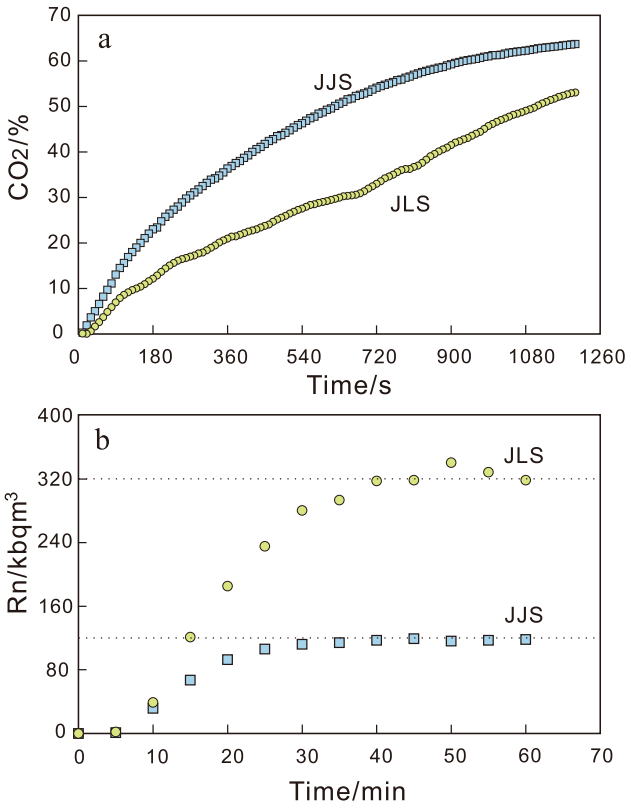

Fig. 4 Variations of CO_2 and Rn concentration with time when conducting flux measurements. **a** Temporal variation of CO_2 concentration. **b** Temporal variation of Rn concentration

Discussion

Deeply derived volatiles from magma reservoirs

In active volcanic regions, magma generally serves as the dominant thermal source and simultaneously supplies substantial volatiles to hydrothermal systems (Stelling et al. 2016; Federico et al. 2002). At Mt. Changbai volcano, comprehensive geophysical investigations have revealed vertically continuous zones of high-conductivity and low-resistivity anomalies extending from mantle to the upper-crust beneath the volcanic cone, indicative of an active magma plumbing system with potential chambers and conduits (e.g., Tang et al. 2014; Zhu et al. 2019; Yang et al. 2021; Fan et al. 2022). The main zone of the uppermost crustal magma chamber is believed to be at about 10–5 km depth below sea level (e.g., Qiu et al. 2014; Hammond et al. 2020). This depth range is corroborated by the predominant focal depth (~ 7.5 km) of seismic swarms recorded during the 2002–2006 volcanic unrest event (Xu et al. 2012). Therefore, the well-developed magmatic plumbing system along with shallow-crustal chambers enable efficient transport of abundant volatiles from deep source to surface at Mt. Changbai volcano.

CO_2 and He are frequently observed in natural fluids on the surface and their isotopic characteristics are widely used to decipher their original sources (Sano and Wakita 1985; Hilton 1996). CO_2 can be generated from multiple geological processes mainly including mantle (magmatic) degassing, metamorphic decarbonization of carbon-bearing rocks, and decomposition of organic matters (e.g., Italiano et al. 2009; Yuce et al. 2014, 2017). As shown in Fig. 5, although CO_2 concentrations vary between samples, the $\delta^{13}C_{CO2}$ values of both JLS and JJS gas samples exhibit comparable ranges, strongly suggesting a predominantly magmatic source for the CO_2. He is typically deriving from three different origins including the mantle, the crust, and the atmosphere. These three origins can be distinguished by the He isotopic values and $^4He/^{20}Ne$ ratios which are ~ 8 Ra (MORB) and > 1000 for mantle, ~ 0.02 Ra and > 1000 for crust, and 1 Ra and 0.318 for atmosphere (Sano and Wakita 1985). Using these end-member compositions, relative He contributions from the three origins can be easily identified. In Fig. 6a, almost all samples plot above the 50% mantle contribution line. Such mantle contributions are quite high considering the crustal and/or air contamination during the upwelling of magma from the mantle to the crust, magma storage in the crustal chambers, and degassed volatiles migration to the

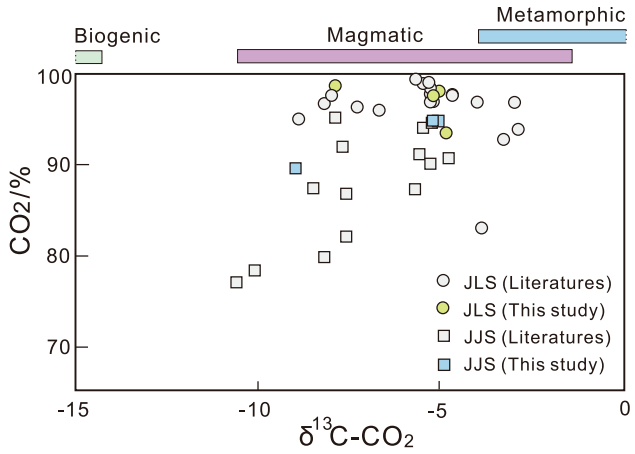

Fig. 5 Scatter plots of CO_2 concentrations versus $\delta^{13}C$-$_{CO2}$ values illustrating the origins of CO_2 in JLS and JJS samples. The three colored boxes represent typical $\delta^{13}C$ ranges of biogenic origin, magmatic origin (Sano and Marty 1995), and metamorphic origin (Holland and Gilfillan 2013). The gray symbols represent data from literatures (Zhang et al. 2015; Wei et al. 2016; Gu et al. 2025)

surface. Compared with JJS, samples from JLS exhibit more He contributions from air. This is consistent with the fact that N_2/O_2 ratios in JLS samples are similar to those in air (Fig. 2b). Applying the ternary mixing model (mantle, carbonate, and organic matter) proposed by Sano and Marty (1995), as shown in Fig. 6b, it can be found that all JLS samples plot within the mixing curves confined by the three end-members, suggesting limited fractionation of CO_2 and He. On the contrary, all JJS samples fall outside the mixing areas because of their relatively low $CO_2/^3He$ ratios. Given that ^3He concentrations show negligible variability, such ratios are dominantly controlled by CO_2 concentration fluctuations. Consequently, the observed $CO_2/^3He$ depletion likely reflects CO_2 removal processes (e.g., calcite precipitation) and/or N_2-induced dilution (Barry et al. 2020; Randazzo et al. 2021). Theoretically, calcite precipitation would cause a negative shift in $\delta^{13}C_{CO2}$ values of the residual phase; however, the JJS samples exhibit $\delta^{13}C_{CO2}$ ranges comparable to JLS (Fig. 5), suggesting calcite precipitation is unlikely to be the primary mechanism. As shown in Fig. 2a, N_2 and CO_2 concentrations of JJS samples show a strong negative correlation. This means the CO_2 of JJS samples can be diluted by N_2, leading to the observed low $CO_2/^3He$ ratios (Fig. 7).

Genesis of degassing differences between JLS and JJS

Although the two groups of hydrothermal springs exhibit similar gaseous C–He isotopic signatures that are typically indicative of magmatic origin, they still present a couple of differences, particularly with regard to the concentration of He, CO_2, and Rn, and the degassing rates of CO_2 and Rn. He is an inert noble gas that separates from magma before soluble gases and would be scarce without the replenishment of fresh magma. CO_2 is the second most abundant volatile (after water vapor) gas dissolved in magma (Pan et al. 1991). Degassing of CO_2 can occur throughout the entire process of magmatism but its intensity would decrease as magma cools down. Thus, the decreased CO_2 flux from magma can be regarded as a symbol of residual degassing (Giammanco et al. 2007). Rn is a radioactive gas and a product from ^{238}U

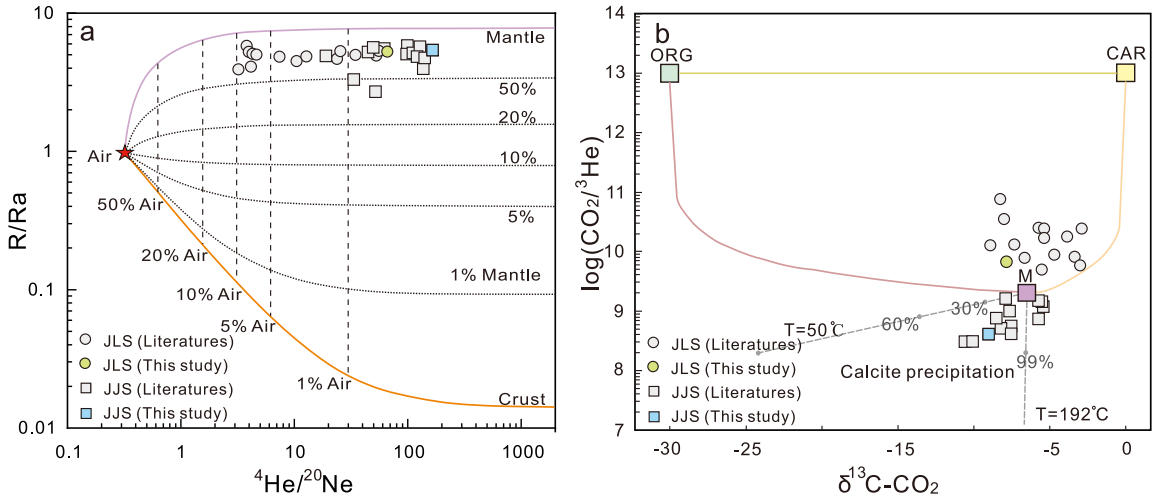

Fig. 6 Ternary mixing models delineating origin of He and CO_2 in gas samples from JLS and JJS. **a** Plots of $^3He/^4He$ (R/Ra) versus $^4He/^{20}Ne$ ratios. R/Ra are 1 for air, 8 for mantle (MORB) and 0.02 for crust; ($^4He/^{20}Ne$) ratios are 0.318 for air, 1000 for mantle and crust (Sano and Wakita 1985). **b** Plots of log ($CO_2/^3He$) versus $\delta 13_{C\text{-}CO2}$ values. The end-member values of mantle (M), carbonate (CAR), and organic matter (ORG) are according to Sano and Marty (1995). The gray symbols represent data from literatures (Zhang et al. 2015; Wei et al. 2016)

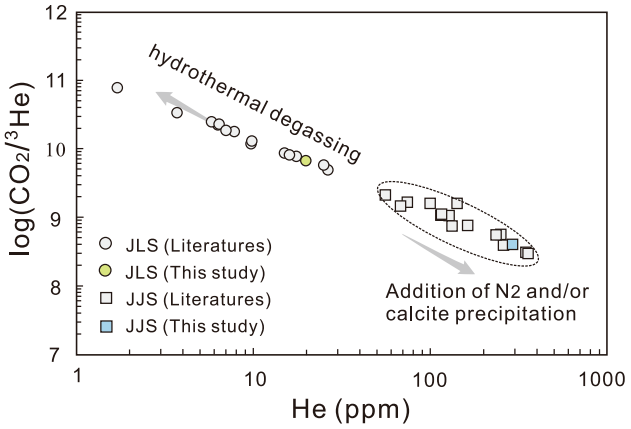

Fig. 7 Plots of He concentrations versus $CO_2/^3He$ ratios showing increasing He concentrations with decreasing $CO_2/^3He$ values. The gray symbols represent data from literatures (Zhang et al. 2015; Wei et al. 2016)

decay series, characterized by a short half-life of 3.82 days. Due to its large atomic weight, Rn has limited diffusion capacity. Consequently, the terrestrial Rn that can be measured comes from the rocks and soil nearby the sampling point. However, when efficient pathways (e.g., fault systems) and carrier gases (primarily CO_2) are available, magma-derived Rn can be effectively transported to the Earth's surface (Etiope and Martinelli 2002; Walia et al. 2005; Yuce et al. 2017). This explains why elevated Rn concentrations are frequently observed in active volcanic regions (e.g., Padilla et al. 2013), where widespread fault networks and abundant magmatic CO_2 facilitate the upward migration of deep-sourced Rn. However, given the short half-life of Rn, this scenario likely requires the magma chamber to be relatively shallow to allow sufficient Rn transport before its radioactive decay.

At Changbai volcano, an intriguing discrepancy is observed between CO_2 concentration and flux at the both springs. JJS displays lower CO_2 concentrations than JLS, yet exhibits approximately three times higher CO_2 flux. Normally, a positive correlation exists between gas concentration and flux because higher concentrations create steeper concentration gradients, thereby promoting gas release from springs. In addition, JLS has higher water temperature which is more inductive for gas escaping, thereby increasing the gas flux. Thus, JLS should theoretically exhibit higher CO_2 flux than JJS, but observed data contradict this expectation. This apparent paradox suggests that there should be additional controlling factors in the degassing dynamics between the two springs, which are originating from either the distinct sources or differential upward migration process. Both the springs are located on the volcanic cone with nearly identical underlying rocks. They have similar circulation depths and have undergone similar water circulation processes (Na et al. 2020). JLS has a little higher water yield than JJS (Gao 2004), suggesting more developed faults or fractures beneath JLS. Collectively, these observations indicate that migration processes exert minimal influence on degassing differences between the two springs. Consequently, inherent distinctions in degassing sources must instead constitute the dominant controlling factor. Unlike CO_2, both Rn concentration and flux are higher at JLS, particularly the Rn concentration, which is over 2.5 times of JJS. Such a substantial disparity is unlikely to be solely caused by surroundings alone. It is highly possible that there is exceed Rn derived from magma at JLS, which means the occurrence of relatively shallow magma sources.

Although geophysical investigations have generally delineated the main zone of the uppermost magma chamber (e.g., Qiu et al. 2014; Hammond et al. 2020), the morphology of its upper boundary remains poorly constrained. Regarding the low-resistivity zones within 5 km depth, some researchers attributed them to saline-bearing geothermal fluids (e.g., Yang et al. 2021), while others propose a magmatic origin (e.g., Zhao et al. 2024). Magma reservoirs in the crust usually play a key role in volcano eruptions (Sparks et al. 1977; Bachmann and Bergantz 2008). Mt. Changbai volcano has large magma reservoirs and has experienced large-scale eruptions since Holocene (Zou et al. 2010; Oppenheimer et al. 2017). Prior to an eruption, ascending magma intrudes into the upper crust, seeking for structure weakness in surrounding rocks and expanding space to store magma. Thus, in addition to the main chamber, there are supposed to be scattered shallow magma pockets at Mt. Changbai volcano. Qiu et al. (2014) conducted a high-resolution magnetotelluric survey crossing the cone of Mt. Changbai and revealed dendritic low-resistivity bodies above the main magma chamber which were likely to represent the magma pockets. It is noteworthy that JLS is located straightly over one of these bodies (Wei et al. 2021). Therefore, based on integrated geochemical and geophysical results, it can be deduced that gases emitted from JLS derives from a shallow magma pocket. During a quiescent stage, this pocket becomes isolated from the main chamber due to lack of magma recharges and the degassing intensity there recede gradually as the magma cools down (Fig. 8). This explains the observed depletion in both He concentration and CO_2 flux at JLS. While at JJS, besides high CO_2 flux, there are also elevated undissolved gas concentrations like N_2 and He, suggesting that its gases originate directly from the main magma chamber, which contains larger volumes of magma and exhibit more extensive magmatism (Fig. 8).

Monitoring strategy based on hydrothermal gas geochemistry

Mt. Changbai volcano is at quiescent stage but retains a fully functional magma plumbing system. The volcanic

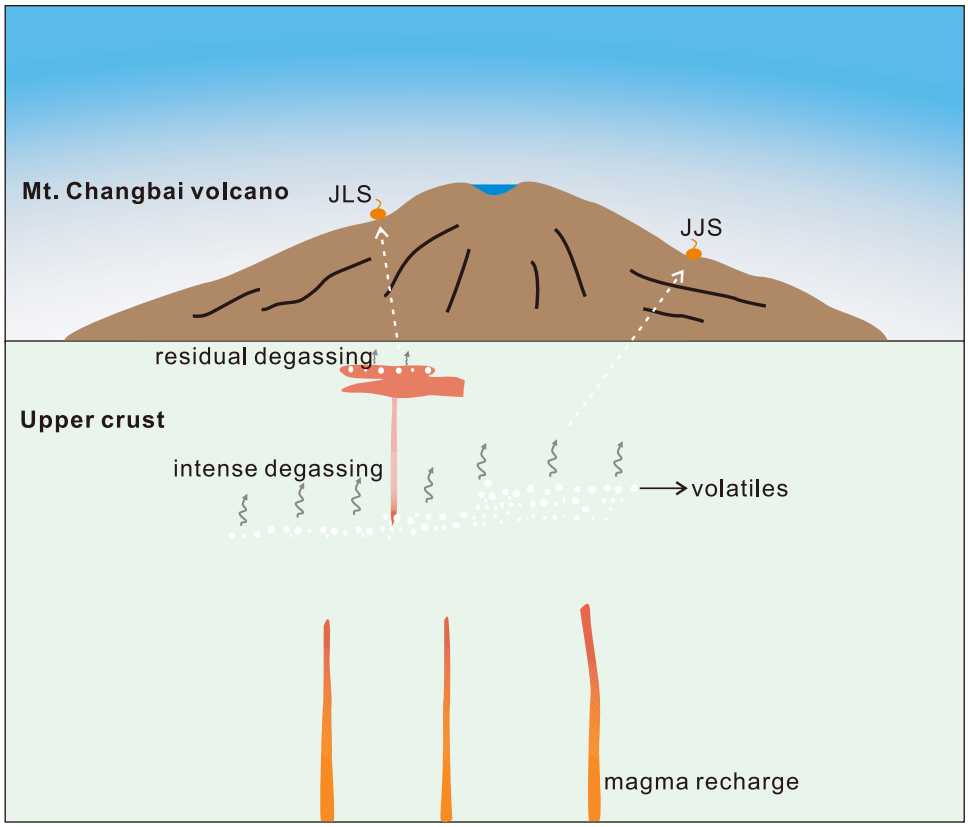

Fig. 8 A conceptual degassing model describing the hydrothermal gas migration from deep magmatic sources to the surface at Mt. Changbai volcano

disturbance during years 2002–2006 stands as a constant reminder of active magmatism and recurrent eruption potential. In addition, Mt. Changbai volcano is vulnerable to the "remote effects" of nearby deep earthquakes associated to plate subduction that may occur at any time (Liu et al. 2017). Therefore, the volcano is still a potential threat to the neighboring communities.

Our study shows that gases from the two hydrothermal springs are governed by deep magmatic degassing, making their geochemical characteristics effective proxies for deep magmatism. However, since they reflect magma sources at distinct depths, different monitoring strategy should be adopted. For JJS, their close association with the main magma chamber makes their geochemical variations critical for detecting abrupt magmatic changes such as magma recharge or fractionation. Key monitoring parameters including CO_2 flux which is a primary indicator of deep magma degassing and undissolved gas concentrations (e.g., He and other noble gases) that can reflect mantle contributions. For JLS, which exhibits residual degassing patterns, they can serve as an effective indicator for assessing the potential ascent of magma within the main chamber. The flux of CO_2 and Rn shall be the suitable monitoring parameters. A sudden increase in CO_2 and Rn flux at JLS would signal upward magma migration, suggesting an elevated risk of volcanic eruption. By conducting joint gas monitoring at JLS and JJS, it is expected to dynamically track the status of deep magmatism beneath Mt. Changbai volcano and determine the urgency of potential eruptions.

Notably, volcanic gas monitoring has been conducted at many volcanoes worldwide, including Mount Etna in Italy (Bruno et al. 2001), the Hawaiian volcanic system in the United States (Kern et al. 2015), and the Canary Islands volcanic complex in Spain (Pérez et al. 2012). Nevertheless, it should be noted that magma storage systems vary significantly among volcanoes. Some volcanoes host multiple shallow magma reservoirs, whereas surface gas degassing patterns are predominantly controlled by their directly connected magma sources (Bruno et al. 2001). Consequently, volcanic gas emissions from different locations may reflect distinct magmatic activities. As the case at Mt. Changbai volcano shows, JLS and JJS exhibit differentiated monitoring capabilities owing to their connections with magma reservoirs at varying depths. Therefore, detailed geochemical investigations must be conducted prior to establishing practical gas monitoring systems.

Conclusion

This study presents the characteristics of concentrations, fluxes, and isotopes of CO_2, Rn, and He emitted from JLS and JJS on the cone of Mt. Changbai volcano, and

investigates their links to volcanic magmatism. The main conclusions are as follows:

(1) JLS and JJS exhibit similar C–He isotopic signatures which are typically of magmatic origin. Gases emitted from the two springs can provide clues related to magmatism.
(2) Excess Rn at JLS is sourced from a shallower magma pocket which is isolated from the main chamber. Depletion in both He concentration and CO_2 flux at JLS can be explained by residual magma degassing. Magmatic CO_2 and He emitted from JJS are mainly derived from the main chamber which hosts larger volumes of magma and exhibit more extensive magmatism.
(3) JLS and JJS can reflect volcanic magmatism at different depths. JJS is closely related to the main magma chamber, their geochemical variations can imply whether there are abrupt changes of magmatic activities in the main magma chamber. JLS, which now shows characteristics of residual degassing, can serve as an effective indicator for assessing the potential ascent of magma within the main chamber. Integrated gas monitoring at both sites would enhance real-time tracking of deep magma dynamics and improve eruption risk assessment. The Changbai volcano case study underscores that comprehensive gas geochemical investigations should precede monitoring applications in volcanic surveillance systems worldwide.

Supplementary Information The online version contains supplementary material available at https://doi.org/10.1007/s00531-025-02520-3.

Acknowledgements We sincerely appreciate the two reviewers and the Editor-in-Chief Ulrich Riller for their valuable comments and constructive suggestions, which have significantly enhanced the quality of this manuscript. This work was funded by the Special Fund of the Institute of Earthquake Forecasting, China Earthquake Administration (Grants CEAIEF20230504), Foundation of Key Laboratory of Petroleum Resources Exploration and Evaluation, Gansu Province (KLPREEGS-2024-17), and National Nonprofit Fundamental Research Grant of China, Institute of Geology, China Earthquake Administration (NORSCBS22-05). The study is a contribution to IGCP-724 project.

Data availability The data that support the findings of this study are available in the Supplementary Information of this article.

Declarations

Conflict of interest The authors declare no conflict of interest.

References

Aiuppa A, Bitetto M, Delle Donne D, La Monica FP, Tamburello G, Coppola D, Schiava MD, Innocenti L, Lacanna G, Laiolo M, Massimetti F, Pistolesi M, Silengo MC, Ripepe M (2021) Volcanic CO_2 tracks the incubation period of basaltic paroxysms. Sci Adv 7(38):eabh0191

Bachmann O, Bergantz G (2008) The magma reservoirs that feed supereruptions. Elements 4(1):17–21

Barry PH, Negrete-Aranda R, Spelz RM, Seltzer AM, Bekaert DV, Virrueta C, Kulongoski JT (2020) Volatile sources, sinks and pathways: a helium–carbon isotope study of Baja California fluids and gases. Chem Geol 550:119722

Bruno N, Caltabiano T, Giammanco S, Romano R (2001) Degassing of SO_2 and CO_2 at Mount Etna (Sicily) as an indicator of pre-eruptive ascent and shallow emplacement of magma. J Volcanol Geotherm Res 110(1–2):137–153

Cassidy M, Mani L (2022) Huge volcanic eruptions: time to prepare. Nature 608(7923):469–471

Chiodini G, Cioni R, Guidi M, Raco B, Marini L (1998) Soil CO_2 flux measurements in volcanic and geothermal areas. Appl Geochem 13(5):543–552

Chiodini G, Paonita A, Aiuppa A, Costa A, Caliro S, De Martino P, Vandemeulebrouck J (2016) Magmas near the critical degassing pressure drive volcanic unrest towards a critical state. Nat Commun 7(1):13712

Etiope G, Martinelli G (2002) Migration of carrier and trace gases in the geosphere: an overview. Phys Earth Planet Inter 129:185–204

Fan XL, Guo Z, Zhao Y, Chen QF (2022) Crust and uppermost mantle magma plumbing system beneath Changbaishan intraplate volcano, China/North Korea, revealed by ambient noise adjoint tomography. Geophys Res Lett 49(12):e2022GL098308

Federico C, Aiuppa A, Allard P, Bellomo S, Jean-Baptiste P, Parello F, Valenza M (2002) Magma-derived gas influx and water–rock interactions in the volcanic aquifer of Mt. Vesuvius, Italy. Geochim Cosmochim Acta 66(6):963–981

Ferres D, Escobar RP, Bowman L (2015) Reflections of volcanologists about their professional role in volcanic risk management in the context of Latin America. Rev Geol Am Cent 52:9–31

Gao QW (2004) Volcanic hydrothermal activities and gas-releasing characteristicsof the Tianchi Lake region, Changbai Mountains. Acta Geosci Sin 25(3):345–350 (**in Chinese with English Abstract**)

Giammanco S, Sims KWW, Neri M (2007) Measurements of ^{220}Rn and ^{222}Rn and CO_2 emissions in soil and fumarole gases on Mt. Etna volcano (Italy): implications for gas transport and shallow ground fracture. Geochem Geophy Geosy 8:Q10001

Gu GH, Hu L, Pan XD, Li Y, Liu ZF, Sun FX, Zhong GP (2025) Hydrogen emission characteristics of Changbaishan Volcano: spatial and temporal distribution and genesis. Geothermics 127:103269

Hammond JOS, Wu JP, Ri KS, Wei W, Yu JN, Oppenheimer C (2020) Distribution of partial melt beneath Changbaishan/Paektu volcano, China/Democratic People's Republic of Korea. Geochem Geophys Geosyst 21(1):e2019GC008461

Hilton DR (1996) The He and carbon isotope systematics of a continental geothermal system: results from monitoring studies at Long Valley caldera (California, USA). Chem Geol 127(1–4):269–295

Holland G, Gilfillan S (2013) Application of noble gases to the viability of CO_2 storage. In: Burnard P (ed) The noble gases as geochemical tracers. Advances in isotope geochemistry. Springer, Berlin, pp 177–223

Huppert HE, Woods AW (2002) The role of volatiles in magma chamber dynamics. Nature 420:493–495

Italiano F, Bonfanti P, Ditta M, Petrini R, Slejko F (2009) Helium and carbon isotopes in the dissolved gases of Friuli region (NE Italy): geochemical evidence of CO_2 production and degassing over a seismically active area. Chem Geol 266:76–85

Kern C, Sutton J, Elias T, Lee L, Kamibayashi K, Antolik L, Werner C (2015) An automated SO_2 camera system for continuous,

real-time monitoring of gas emissions from Kīlauea Volcano's summit Overlook Crater. J Volcanol Geotherm Res 300:81–94

Kim S, Tkalčić H, Rhie J (2017) Seismic constraints on magma evolution beneath Mount Baekdu (Changbai) volcano from transdimensional Bayesian inversion of ambient noise data. J Geophys Res Solid Earth 122(7):5452–5473

Liu G, Li C, Peng Z, Li X, Wu J (2017) Detecting remotely triggered microseismicity around Changbaishan Volcano following nuclear explosions in North Korea and large distant earthquakes around the world. Geophys Res Lett 44(10):4829–4838

Liu ZF, Chen Z, Li Y, Zhao ZD, Sun AH, Li JC, Dong JY, Zhao Y, Hu L, Gao ZH, Lu C, Su SJ, He HY, Zhao YX (2024) Crust uplift controls the massive emissions of 222Rn and CO_2 in the Northeastern Tibetan Plateau. China Chem Geol 663:122280

Mamyrin BA, Tolstikhin IN (1984) Helium isotopes in nature. Developments in geochemistry. Elsevier, Amsterdam, p 273

Mangler MF, Petrone CM, Prytulak J (2022) Magma recharge patterns control eruption styles and magnitudes at Popocatépetl volcano (Mexico). Geology 50:366–370

Na J, Yan BZ, Chi BM, Feng B, Jiang X (2020) The estimation of reservoir temperature for thermal springs using the integrated multicomponent geothermometry method at Changbai Mountain, Northeastern Songliao Basin, China. Geofluids 1:6418215

Oppenheimer C, Wacker L, Xu J, Galvan JD, Stofel M, Guillet S, Corona C, Sigl M, Di Cosmo N, Hajdas I, Pan B, Breuker R, Schneider L, Esper J, Fei J, Hammond J, Buntgen U (2017) Multiproxy dating the 'Millennium Eruption' of Changbaishan to late 946 CE. Quat Sci Rev 158:164–171

Padilla GD, Hernández PA, Padrón E, Barrancos J, Pérez NM, Melián G, Hernández I (2013) Soil gas radon emissions and volcanic activity at El Hierro (Canary Islands): the 2011–2012 submarine eruption. Geochem Geophys Geosyst 14(2):432–447

Pan V, Holloway JR, Hervig RL (1991) The pressure and temperature dependence of carbon dioxide solubility in tholeiitic basalt melts. Geochim Cosmochim Acta 55(6):1587–1595

Pan B, de Silva SL, Xu JD, Liu SJ, Xu D (2020) Late pleistocene to present day eruptive history of the Changbaishan-Tianchi volcano, China/Dprk: new field, geochronological and chemical constraints. J Volcanol Geotherm Res 399:106870

Patanè D, De Gori P, Chiarabba C, Bonaccorso A (2003) Magma ascent and the pressurization of Mount Etna's volcanic system. Science 299:2061–2063

Pérez NM, Padilla GD, Padrón E, Hernández PA, Melián GV, Barrancos J, Hernández Í (2012) Precursory diffuse CO_2 and H_2S emission signatures of the 2011–2012 El Hierro submarine eruption, Canary Islands. Geophys Res Lett 39(16):L16311

Qiu GG, Fei FG, Fang H, Du BR, Zhang XB, Zhang PH, Yuan YZ, He MX, Bai DW (2014) Analysis of magma chamber at the Tianchi volcano area in Changbai mountain. Chin J Geophys 57(10):3466–3477 (**in Chinese with English Abstract**)

Randazzo P, Caracausi A, Aiuppa A, Cardellini C, Chiodini G, D'Alessandro W, Li Vigni L, Papic P, Marinkovic G, Ionescu A (2021) Active degassing of deeply sourced fluids in central Europe: new evidences from a geochemical study in Serbia. Geochem Geophys Geosyst 22:e2021GC010017

Ruprecht P, Bachmann O (2010) Pre-eruptive reheating during magma mixing at Quizapu volcano and the implications for the explosiveness of silicic arc volcanoes. Geology 38:919–922

Sano Y, Marty B (1995) Origin of carbon in fumarolic gas from island arcs. Chem Geol 119:265–274

Sano Y, Wakita H (1985) Geographical distribution of $^3He/^4He$ ratios in Japan: implications for arc tectonics and incipient magmatism. J Geophys Res 90(B10):8729–8741

Sparks SR, Sigurdsson H, Wilson L (1977) Magma mixing: a mechanism for triggering acid explosive eruptions. Nature 267(5609):315–318

Stelling P, Shevenell L, Hinz N, Coolbaugh M, Melosh G, Cumming W (2016) Geothermal systems in volcanic arcs: volcanic characteristics and surface manifestations as indicators of geothermal potential and favorability worldwide. J Volcanol Geotherm Res 324:57–72

Tang Y, Obayashi M, Niu F, Grand SP, Chen YJ, Kawakatsu H, Tanaka S, Ning J, Ni JF (2014) Changbaishan volcanism in northeast China linked to subduction-induced mantle upwelling. Nat Geosci 7(6):470–475

Tilling RI (2008) The critical role of volcano monitoring in risk reduction. Adv Geosci 14:3–11

Walia V, Su TC, Fu CC, Yang TF (2005) Spatial variations of radon and helium concentration in soil gas across Shan-Chiao fault, Northern Taiwan. Radiat Meas 40:513–516

Wei H, Liu G, Gill J (2013) Review of eruptive activity at Tianchi volcano, Changbaishan, northeast China: implications for possible future eruptions. Bull Volcanol 75(1):1–14

Wei FX, Xu JD, Shangguan ZG, Pan B, Yu HM, Wei W, Bai X, Chen ZQ (2016) Helium and carbon isotopes in the hot springs of Changbaishan Volcano, northeastern China: A material connection between Changbaishan Volcano and the west Pacific plate?. J Volcanol Geothermal Res 327:398–406

Wei FX, Xu JD, Kong QJ, Liu SJ, Xu D, Pan B (2021) Sources of CH_4 with variable carbon isotopes from Changbaishan volcano in NE China: implications for the feeding system. J Volcanol Geotherm Res 419:107355

Xu JD, Liu GM, Wu JQ, Ming YH, Wang QL, Cui DX, Shangguan ZG, Pan B, Lin XD, Liu JQ (2012) Recent unrest of Changbaishan volcano, northeast China: a precursor of a future eruption? Geophys Res Lett 39(16):L16305

Yan BZ, Liang XJ, Xiao CL (2018) Hydrogeochemical characteristics and genesis model of Jinjiang and Julong hot springs in Changbai Mountain, Northeast China. Geofluids 1:1694567

Yang B, Lin W, Hu X, Fang H, Qiu G, Wang G (2021) The magma system beneath Changbaishan-Tianchi Volcano, China/North Korea: constraints from three-dimensional magnetotelluric imaging. J Volcanol Geotherm Res 419:107385

Yuce G, Italiano F, D'Alessandro W, Yalcin TH, Yasin DU, Gulbay AH, Ozyurt NN, Rojay B, Karabacak V, Bellomo S, Brusca L, Yang T, Fu CC, Lai CW, Ozacar A, Walia V (2014) Origin and interactions of fluids circulating over the Amik Basin (Hatay-Turkey) and relationships with the hydrologic, geologic and tectonic settings. Chem Geol 388:23–39

Yuce G, Fu CC, D'Alessandro W, Gulbay AH, Lai CW, Bellomo S, Yang TF, Italiano F, Walia V (2017) Geochemical characteristics of soil radon and carbon dioxide within the Dead Sea Fault and Karasu Fault in the Amik Basin (Hatay), Turkey. Chem Geol 469:129–146

Zhang ML, Guo ZF, Sano Y, Cheng ZH, Zhang LH (2015) Stagnant subducted Pacific slab-derived CO_2 emissions: Insights into magma degassing at Changbaishan volcano, NE China. J Asian Earth Sci 106:49–63

Zhang ML, Guo ZF, Liu JQ, Liu GM, Zhang LH, Lei M, Zhao WB, Ma L, Sepe V, Ventura G (2018) The intraplate Changbaishan volcanic field (China/North Korea): a review on eruptive history, magma genesis, geodynamic significance, recent dynamics and potential hazards. Earth Sci Rev 187:19–52

Zhao R, Shan X, Wu C, Yi J, Hao G, Wang P (2019) Formation and evolution of the Changbaishan volcanic geothermal system in a convergent plate boundary back-arc region constrained by boron isotope and gas data. J Hydrol 569:188–202

Zhao LQ, Zhan Y, Kiyan D, Xu JD, Hu YX, Tang J, Sun XY, Wang QL, Cao C (2024) Magnetotelluric evidence for the deep causes of different eruptive styles of Changbaishan Tianchi and Longgang volcanoes. Sci Rep 14(1):24897

Zhu HX, Tian Y, Zhao DP, Li HH, Liu C (2019) Seismic structure of the Changbai intraplate volcano in ne China from joint inversion of ambient noise and receiver functions. J Geophys Res Solid Earth 124(5):4984–5002

Zou H, Fan Q, Zhang H (2010) Rapid development of the great Millennium eruption of Changbaishan (Tianchi) Volcano, China/North Korea: evidence from U–Th zircon dating. Lithos 119(3–4):289–296